INTERMEDIATE RANGE ORDER, DEFECTS AND THERMAL RELAXATION IN SILICA

Frank L. Galeener
Department of Physics
Colorado State University
Fort Collins, CO 80523, USA

Abstract

This paper provides a brief description of the effects of fictive temperature T_F and hydroxyl concentration [OH] on the short and intermediate range structure of vitreous SiO_2. Earlier Raman spectroscopy and electron spin resonance studies by the author and his collaborators are reviewed, and some recently acquired T_F-dependent X-radioluminescence data are presented.

I. Introduction

It is well known that certain properties of pure vitreous (v−) SiO_2 depend on the thermal history of the sample. If the thermal history is appropriately controlled, its effects can be characterized by a fictive temperature T_F [1]. The idea is that a glassy sample with a well−defined fictive temperature has a statistically well−defined structure. Many examples of the dependence of properties on T_F have been discussed elsewhere, notably by Bruckner [2] and Primak [3]. It is also well known [4] that certain properties are quite sensitive to modest levels of OH impurities: Thus, the viscosity of v−SiO_2 is reduced by three orders of magnitude at ~1000°C when the (otherwise pure) material contains ~1200 ppm hydroxyl concentration [OH].

In this paper I will review the T_F and [OH] dependencies of the network and defect structure of v−SiO_2, as revealed by our studies of Raman spectra [5−7], and our studies of x−ray induced electron spin resonance (ESR) [8,9] and optical luminescence [10]. These studies access information about the structure at both short and intermediate ranges.

Elsewhere, Galeener [11−13] has given careful definitions of the four ranges of order in an amorphous solid: short, intermediate, long and global. We shall here discuss only the first two ranges.

Short range order (SRO) describes the nearest neighbor bonding environment of each atomic species. The elements of SRO in the idealized perfect continuous random network model for v−SiO_2 can be visualized with the help of Fig. 1, where one can see schematically the

SRO around the Si and that around the O atomic species, both specified in the caption. In our definition of SRO, all neighbors of a species are treated as if they are *spherically symmetric*. This allows logical separation of SRO from intermediate range order (which recognizes that the neighbors are *not* spherically symmetric, and have bonding orientations associated with them).

While Fig. 1 and its caption define the SRO of the idealized SiO_2 glass network, it does not show the SRO of possible defects in the network. Figure 2 shows the SRO of the three point defects assigned to the three "intrinsic" ESR signals reported in v-SiO_2 [14-16].

Figure 2(a) shows a defect structure where a Si atom is bonded to only three oxygen atoms, each of which is connected properly to the rest of the network. The unbonded sp^3 orbital is shown as containing a single electron with spin indicated by the arrow. This spin will exhibit ESR and is identified [17] with the spectral signature called the E' line. It is thought that this structure is usually accompanied by a second 3-bonded Si atom which has relaxed into the plane of its three oxygen atoms, and in that case the structure is referred to as an oxygen vacancy. Should the sp^3 orbital lose its electron or capture another, there will be no net spin at the site and no E' signal. We take the strength of the E' line to measure the number of Si atoms which have one net electron spin and are bonded to three oxygen atoms in a trigonal pyramidal configuration like that shown in Fig. 2(a).

Figure 2(b) depicts the non-bridging oxygen hole center (NBOHC) whose spin signal was identified by Stapelbroek et al. [18] in v-SiO_2 containing substantial concentrations of -OH, so called "wet" material. We take the strength of the NBOHC ESR line to measure the number of

dangling oxygen atoms that have trapped a hole and exhibit a spin, as depicted in Fig. 2(b).

Figure 2(c) shows the peroxyl radical hole center (PRHC) whose spin signal was identified by Frieble et al. [19] in v−SiO_2 containing very little or no −OH units, so called "dry" material. We take the strength of the PRHC ESR line to measure the number of dangling peroxyl radicals that have trapped a hole and exhibit a spin, as depicted in Fig. 2(c).

Intermediate range order (IRO) involves specification of relative atomic positions over several nearest neighbor distances, given the SRO. Most fundamentally, it recognizes that nearest neighbors are usually not spherically symmetric. IRO may take the form of specification of the dihedral angles δ,Δ shown in Fig. 1, distributions of their values, etc. Figure 3 shows two special cases of IRO in the form of regular rings of Si−O bonds: (a) is a planar 3−ring and (b) represents a regular puckered 4−ring. (An n−ring has n SiO_4 tetrahedra.) The Raman signals corresponding to these network structures were identified by Galeener and coworkers [20−23] in both "wet" and "dry" v−SiO_2. The planar 3−ring corresponds to the D_2 (606 cm^{-1}) line and the regular 4−ring to the D_1 (495 cm^{-1}), where both lines are shown in Fig. 4. Recent extensive modeling of the vibrations of these rings [23] supports the original assignments [20]. We take the strength of D_2 in a Raman spectrum to measure the concentration of planar 3−rings, as depicted in Fig. 3(a). The strength of D_1 measures the concentration of regular puckered 4−rings, like that illustrated in Fig. 3(b) and discussed in Ref. [23].

While the n−rings are examples of IRO in the undefected network of the glass, one can also give examples of IRO associated with spin active defects. Specification of the relative positions of the atoms in an oxygen vacancy as earlier defined involves specification of IRO. The

IRO of the defect would clearly depend on the SRO around the second Si atom (whether or not the second Si atom relaxed into the plane of its three nearest neighbor oxygen atoms) and on the arrangement of nearby Si–O bonds connecting the two Si atoms. To my knowledge, there is no information concerning the IRO of the E′ defect *in* v–SiO_2, other than the belief that the second Si has relaxed into the plane of its oxygen atoms [17].

II. Dependence of Network Structure and Relaxation Rates on T_F and [OH]

Figure 4 shows the room temperature HH polarized Raman spectra of v–SiO_2 for samples with fictive temperatures 1500°C (a) and 1000°C (b). It is clear that the areas under the sharp D_1 and D_2 lines have changed. Not so clear is the fact [7] that the four peak frequencies marked ω_i have also changed, while the areas under those peaks have not. Also not shown is the fact [7] that the peak positions and areas of all six marked lines do not measurably depend on [OH] up to [OH] ~1200 ppm.

Geissberger and Galeener [7] have reported the T_F dependencies of the frequencies of the six lines, as shown in Fig. 5. The straight lines drawn are least–squares fits to the data. As explained elsewhere [24,25], the four broad features ω_i can be understood quantitatively in terms of a continuous random network of SiO_4 tetrahedra making Si–O–Si bond angles θ and having *no* specific IRO. Thus the positions and shifts of the ω_i tell us almost exclusively about the average SRO in the glass. The fact that ω_1 and ω_3 increase with T_F while ω_4(TO) and ω_4(LO) decrease, is consistent with a model in which there is no change in the tetrahedral arrangement of O atoms about Si, while the average value of θ decreases by ~2° from T_F = 900°C to T_F = 1550°C. We conclude that the

tetrahedra are brought closer together as T_F increases, and this is consistent with the known densification [3] as T_F rises. Moreover, we have a quantitative measure ($\Delta\theta \simeq -2°$) of the extent of change in network *SRO only*, while densification reflects possible changes of structure at *all* ranges of order.

The fact that the position of D_2 does not change with T_F tells us that both SRO and IRO in the planar 3-rings remain unchanged. The small but noticeable increase in the position of D_1 with T_F is consistent with increased puckering of the four rings in which $\Delta\theta \simeq -2°$ [26]. In general, variation in the peak vibrational *frequencies* of v-SiO_2 with T_F gives quantitative information about changes in *SRO*.

We will next show that the changes in the *strengths* of D_1 and D_2 give information about changes in the *IRO of the glass*. Figure 6 shows that the fraction of HH spectral area under D_2 varies in Arrhenius fashion with an energy of formation of 0.44 ± 0.04 eV [6]. The Arrhenius curve is the same for "wet" and "dry" samples and almost the same for all fluorine concentrations [F] up to about 5% (shown). In fact *both* D_2 and D_1 concentrations are independent of OH concentrations up to at least [OH] ~1200 ppm.

Figure 7 shows careful data on the fractional areas under D_1 and D_2 in high purity "dry" v-SiO_2, as reported in Ref. [7]. The energies of formation ("activation energies") shown in Fig. 7 are close to those calculated by O'Keeffe and Gibbs [27] for 3- and 4-rings, using ab-initio quantum mechanical methods. This agreement adds conviction to the original assignments of Galeener [20], and confirms that D_1 and D_2 represent elements of special IRO in the glass. Thus the strengths of D_1 and D_2 give quantitative information about the changes in *regular ring*

IRO with T_F. We presently have no way of using vibrational spectra to learn about other aspects of IRO in such glasses.

It is essential to mention one more aspect of such measurements. The time required for the fractional area under D_1 or D_2 to come to a steady state value at a given annealing temperature T_A is highly dependent on both T_A and impurity content. Some numerical details are given in Ref. [7]. The behavior is illustrated schematically in Fig. 8, where the behavior is explained in the caption. For example, beginning with equilibration of a "wet" and somewhat impure v−SiO_2 sample at T_O = 1200°C, new equilibration at T_A = 1000°C required ~7 hours whereas new equilibration at T_A = 810°C required ~9 days [7]. The times are much longer for "dry" high purity material. It is for this reason that low T_A data in Fig. 6 were obtained on samples with high concentrations of the network terminator fluorine - in order to attain equilibrium in practical periods of time.

It is clear that a well defined T_F requires attention to these equilibration times. We have established equilibration times for D_1 and D_2 [7] and simply assume these times are adequate for a well defined T_F. However, it may be that some other length of time is required to equilibrate a different aspect of structure, and we shall note this possibility in our discussion of defects. True T_F would require that *all* aspects of structure come to a (metastable) steady state.

Finally, we note that a change in the concentration of planar 3−rings, for example, seems to require a rather complex restructuring, possibly the breaking of bonds in two larger rings followed by bond or atom migration, then rebonding and relaxation to planarity. That this can take place in v−SiO_2 at temperatures as low as 700°C [cf. Fig. 6] when melting is at T_M ~ 1700°C and the glass transition is at

T_G ~ 1200°C is remarkable. A seemingly simple process for forming 3-rings at internal surfaces in porous SiO_2 has been suggested by Brinker et al. [28], and a similar mechanism might play some role in our (nominally non-porous) bulk glass samples.

III. Dependence of Point Defect Concentrations and Formation Rate on T_F and [OH]

It is well known that pure v-SiO_2 which has been quenched at normal rates shows no detectable ESR signal [14-16]. This absence of unpaired spins in pristine material is also true for otherwise pure material containing the ubiquitous -OH impurity. ESR signals are observed only after exposure to various additional disturbances, including neutrons, ions, electrons, γ-rays and x-rays. We have engaged in a dose-dependence study of the production of spin signals in v-SiO_2 by irradiation with x-rays [8-10].

Figure 9 shows the increase in E' spin signal strength S with x-ray exposure time t, for "wet" high purity v-SiO_2, containing [OH] ~ 1200 ppm. The x-rays are all of those emitted by a Cu-target tube operated at about 40 keV and having a thin beryllium window, hence x-ray photon energies are in the range 3 keV $\leq h\nu \leq$ 40 keV. Experimental details will be given in a forthcoming paper [9]. We note that 100 hours of exposure corresponds to a dose of about 250 Mrad (SiO_2). The number of spins in the sample increases linearly with dose, just as one might initially expect. The rate of increase is noticeably greater for T_F = 1350°C than for T_F = 700°C. That is, under x-irradiation material with a lower fictive temperature is more radiation hard with respect to creation of E' defects.

Figure 10 shows the result of a similar experiment on "dry" pure v-SiO_2, containing less than 2 ppm -OH. The curves are now non-linear with dose! At any dose, a change in T_F has a much greater fractional effect on the total spin signal S than was the case for -OH containing material. The slopes at high dose are smaller than they were for "wet" material, so at even higher doses "dry" material annealed to low T_F will be significantly more radiation hard than "wet" material.

As described elsewhere [5-7] we interpret this non-linear behavior to be the sum of two processes: (1) a linear increase in spin signal due to creation of *new* defects and (2) an exponentially saturating increase in spin signal due to x-ray induced trapping of electrons on preexisting defects. We refer to the processes as (1) "creation" and (2) "activation" of defects by irradiation. With this interpretation, linear projection of the high dose data to zero dose measures the number of preexisting defect sites. That is, the zero dose intercepts of the dashed lines in Fig. 10 show that the number of preexisting E' defects (or oxygen vacancies) in a "dry" sample with T_F = 1350°C is about twice that in one with T_F = 1000°C. Moreover, on the same scale of S, "wet" material has *no* preexisting E' defects!

Figure 11 shows similar non-linear behavior for the NBOHC defect, the hole-like (H-) center seen in "dry" material. These dose curves are also interpreted in terms of the two processes, "creation" and "activation," where activation now involves trapping of a hole.

In Ref. [9] numerical values are tabulated for the intercepts, slope, etc. Inspection of Figs. 9-12 will affirm the general conclusion: The number of preexisting defects depends strongly on both [OH] and T_F, as does the rate of creation of new defects with x-ray bombardment. Not so obvious is the fact that there are [OH] and T_F

dependencies of the *rate* at which preexisting defects are "activated" by increasing x-ray dose. Moreover, the dependencies are numerically different for each kind of defect, E', NBOHC and PRHC.

Having shown that the rate of production of ***spin signals*** varies strongly with T_F, [OH] and defect type, we will show that ***luminescence*** signals are also dependent on these parameters, in somewhat different ways.

In recent work, Kerwin and Galeener [10] have monitored the intensity of the 2.7 eV luminescence line emitted by v-SiO_2 *while* it is under bombardment by the Cu-tube x-rays. The results versus dose for various T_F are shown in Fig. 13 for "wet" material and in Fig. 14 for "dry" material.

At present we interpret these curves in terms of three processes: (1) a linear increase due to "creation" of new centers involved in the luminescence transition; (2) an abrupt rise in less than 0.1 Mrad (SiO_2 of dose); followed by (3) a perhaps exponential decay with dose to the straight line caused by process (1). We find that the slopes of the straight lines depend somewhat on [OH] but not on T_F. The intercepts depend strongly on T_F but *not* on [OH]. This suggests that the 2.7 eV luminescence transition may not involve any of the three ESR active defects that we have studied (since their preexisting concentration depended strongly on [OH]). In general Fig.s 13 and 14 show that the x-radioluminescence of v-SiO_2 at 2.7 eV depends on both T_F and [OH].

Finally we note that the Raman active defects corresponding to D_1 or D_2 cannot be the same as any one of the three spin active defects, because the [OH] dependencies do not match. The equilibrium concentrations of D_2 (and D_1) are independent of [OH] (see Fig. 6), contrary to the concentrations of the spin active defects. It is also

possible to argue [9] that the D_1 and D_2 defects are not preferential precursor sites for x-ray formation of any one of the three spin active defects.

IV. Concluding Remarks

We have demonstrated that Raman spectroscopy as well as x-ray induced ESR and luminescence spectroscopies reveal T_F and [OH] dependencies of both SRO and special aspects of IRO in v-SiO_2. Much of the same can be accomplished in other glasses, in principle.

The author is grateful to the organizers and sponsors of the conference for their invitation to attend and for their hospitality. He is also grateful to the U.S. Navy Office of Naval Research (G. B. Wright) for partial support of this work.

References

1. See, e.g., R. H. Doremus, Glass Science (Wiley, New York, 1973).

2. R. Bruckner, J. Non-Crystalline Solids 5, 123 (1970).

3. W. Primak, The Compacted States of Vitreous Silica (Gordon and Breach, New York, 1975).

4. Ref. 1, p. 105.

5. F. L. Galeener, J. C. Mikkelsen Jr. and N. M. Johnson, in The Physics of SiO_2 and Its Interfaces, ed. S. T. Pantelides (Pergamon, New York, 1978) p. 284.

6. J. C. Mikkelsen, Jr. and F. L. Galeener, J. Non-Crystall. Solids 37, 71 (1980).

7. A. E. Geissberger and F. L. Galeener, Phys. Rev. B28, 3266 (1983).

8. F. L. Galeener and J. C. Mikkelsen, Jr., in Induced Defects in Insulators, ed. P. Mazzoldi (les editions de Physique, Paris, 1985) p. 141.

9. F. L. Galeener, D. B. Kerwin and J. C. Mikkelsen, Jr., submitted to Phys. Rev. B.

10. D. B. Kerwin and F. L. Galeener, unpublished.

11. F. L. Galeener, Diffusion and Defect Data 53-54, 305 (1987).

12. F. L. Galeener, J. Non-Crystall. Solids 123, 182 (1990).

13. F. L. Galeener, in Disorder in Condensed Matter Physics, eds. J. Blackman and J. Taguena (Oxford University Press, Oxford, 1990) p. 45.

14. D. L. Griscom, this volume.

15. D. L. Griscom, J. Non-Crystall. Solids 40, 211 (1980).

16. D. L. Griscom, J. Non-Crystall. Solids 31, 241 (1978).

17. F. J. Feigl, W. B. Fowler and K. L. Yipp, Solid State Commun. 14, 225 (1974).

18. M. Stapelbroek, D. L. Griscom, E. J. Friebele and G. H. Sigel, Jr., J. Non-Crystall. Solids 32, 313 (1979).

19. E. J. Friebele, D. L. Griscom, M. Stapelbroek and R. A. Weeks, Phys. Rev. Lett. 42, 1346 (1979).

20. F. L. Galeener, Solid State Commun. 44, 1037 (1982).

21. F. L. Galeener, R. A. Barrio, E. Martinez and R. J. Elliott, Phys. Rev. Lett. 53, 2429 (1984).

22. F. L. Galeener, in the Physics of Disordered Materials, eds. D. Adler, H. Fritzsche and S. R. Ovshinsky (Plenum, New York, 1985) p. 159.

23. F. L. Galeener, R. A. Barrio, E. Martinez and R. J. Elliott, submitted to Phys. Rev. B.

24. F. L. Galeener, Phys. Rev. B19, 4292 (1970).

25. F. L. Galeener and G. Lucovsky, Phys. Rev. Lett. 37, 1474 (1976).

26. F. L. Galeener, unpublished.

27. M. O'Keeffe and G. V. Gibbs, J. Chem. Phys. 81, 876 (1984).

28. C. J. Brinker, D. R. Tallant, E. P. Roth and C. S. Ashley, in Defects in Glasses, eds. F. L. Galeener, D. L. Griscom and M. J. Weber (Mat. Res. Society, Pittsburgh, 1986) p. 387.

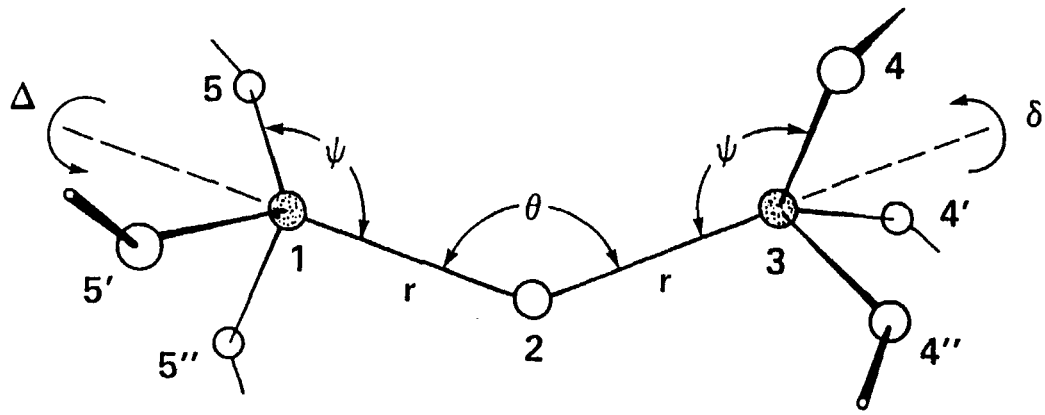

Fig. 1. The relative orientation of two corner sharing tetrahedra in v−SiO_2, showing the short range order and one aspect of the intermediate range order. The Si atoms (dark) are surrounded tetrahedrally at distance r by four O atoms and each O atom bridges between two Si atoms with an angle θ that varies from site to site. This specifies the SRO. The dihedral angles δ,Δ, giving the angular orientation of tetrahedra about their bridging O−Si bonds, are defined to be elements of IRO.

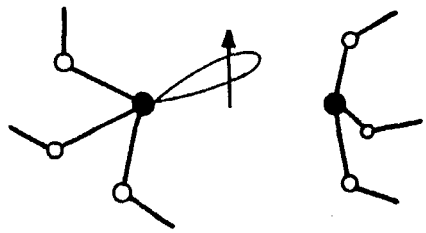

(a) E-PRIME ELECTRON CENTER

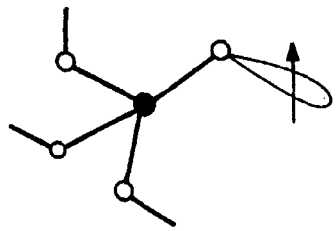

(b) NON-BRIDGING OXYGEN HOLE CENTER

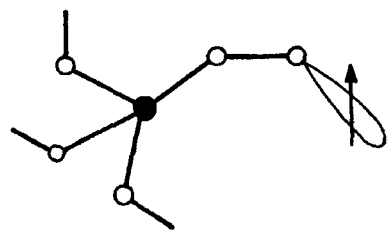

(c) PEROXYL RADICAL HOLE CENTER

Fig. 2. The three spin-active defects in v-SiO_2, for which spin signals have been identified. Each of these involves broken bonds, as shown.

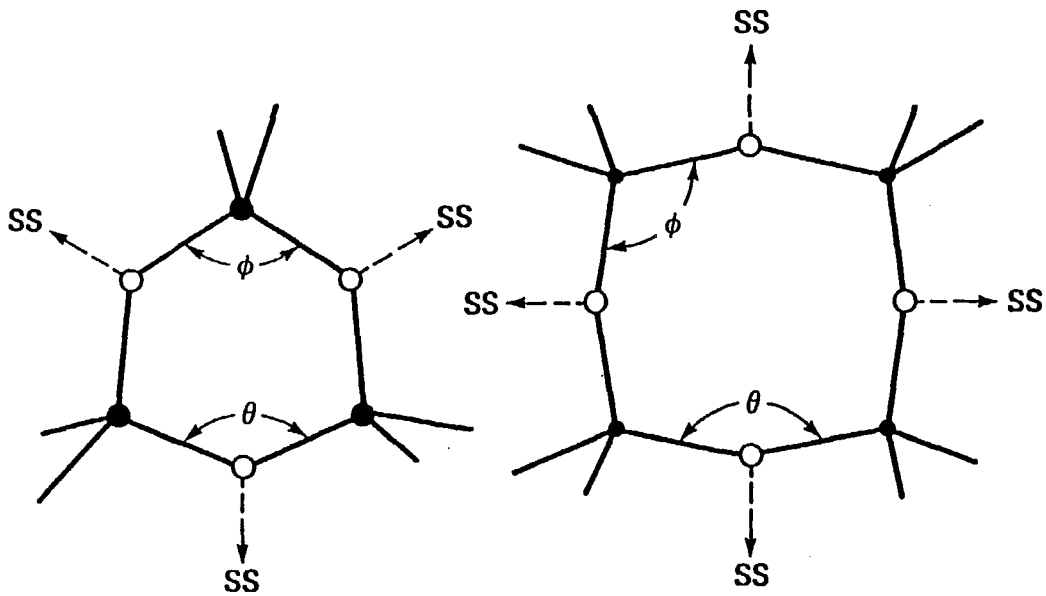

(a) PLANAR 3-FOLD RING (b) PUCKERED 4-FOLD RING

Fig. 3. The two regular ring "defects" in v−SiO_2, for which Raman signatures have been identified. These do not involve broken bonds and are "defects" only in the sense that they are sites of greater regularity in an otherwise more disordered glass network. The bonds external to the rings connect through oxygen atoms to the rest of the network. SS indicates the symmetric stretch motions of the oxygen atoms in the breathing mode of each ring.

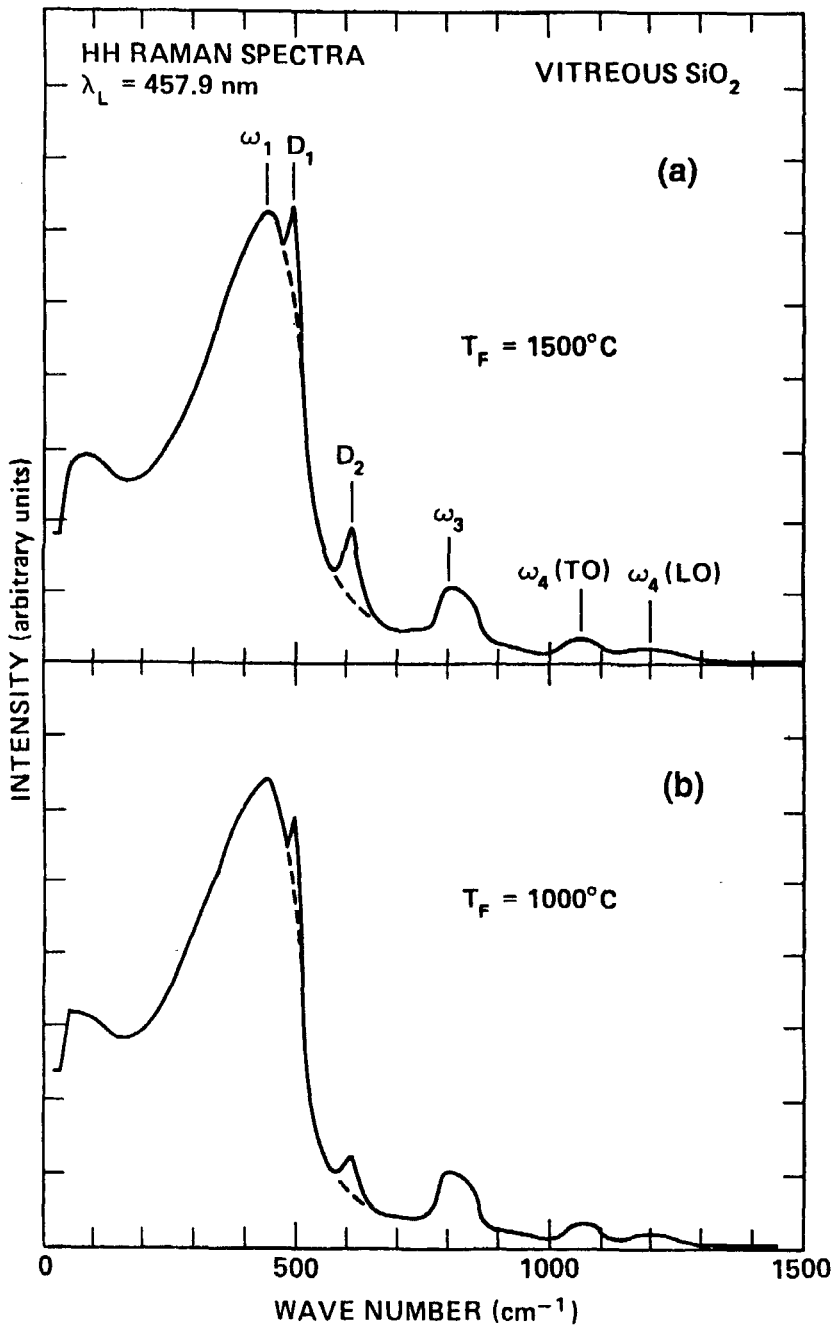

Fig. 4. Two HH polarized Raman spectra [(a) T_F = 1500°C and (b) T_F = 1000°C] of v−SiO_2 showing the changes due to different fictive temperatures T_F. Features labeled ω_i have been identified with vibrations of the v−SiO_2 continuous random network, while features labeled D_i have been associated with regular ring defects. Dashed lines below the D_i features are typical baselines used in the area measurements given in Fig. 6 and 7.

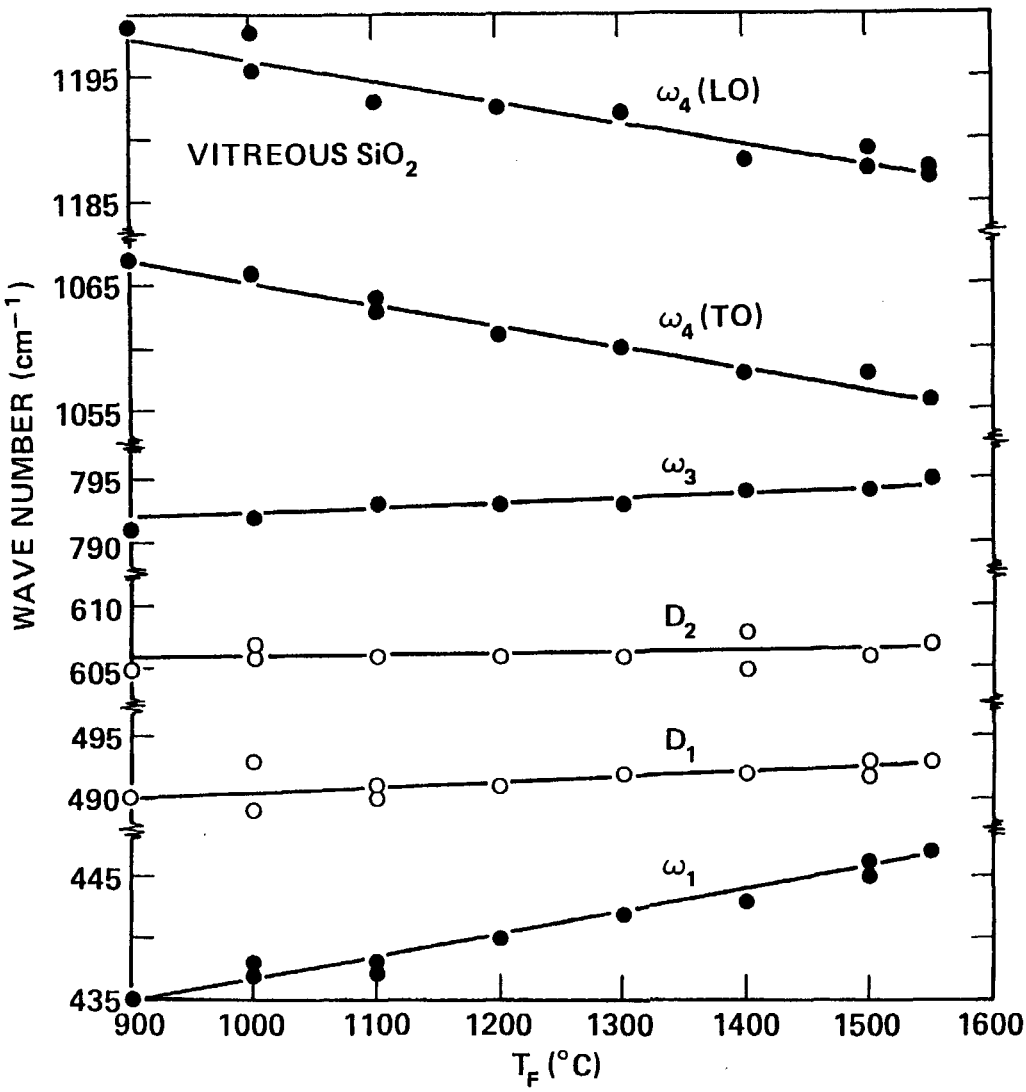

Fig. 5. Plot of the peak positions of the Raman features as a function of T_F. Lines drawn through the points are least-squares fits to the data. Note that the values of ω_1 and ω_3 increase with increasing T_F while those of ω_4 (TO and LO) decrease, as predicted by a simple continuous random network theory. The values for D_2 are unchanged, as befits the planar 3-ring shown in Fig. 3(a); those for D_1 increase slightly and this is consistent with the regular puckered 4-ring depicted in Fig. 3(b).

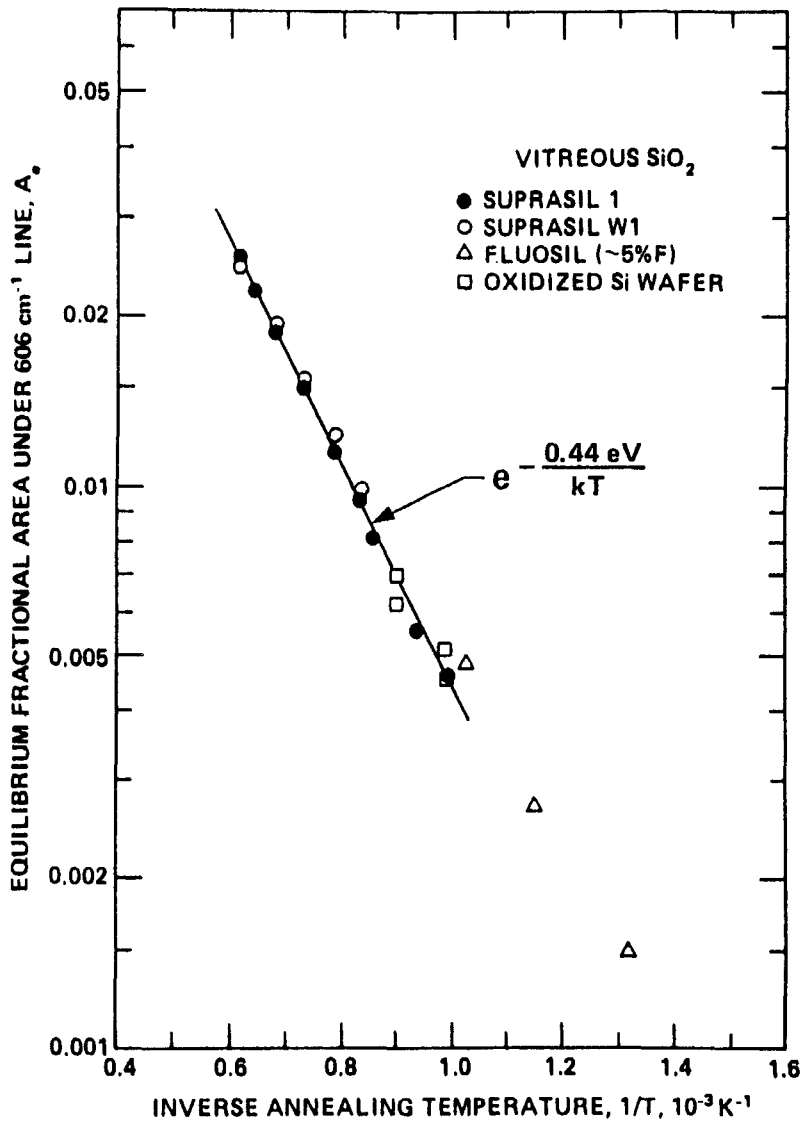

Fig. 6. Semilogarithmic plot of the fractional area under the D_2 (606 cm^{-1}) sharp Raman line in v−SiO_2 containing various amounts of −OH and −F. Note that all points lie on nearly the same Arrhenius curve independent of [OH] and [F]. That is, when annealed to equilibrium at T_F, the [D_2] is independent of [OH]. Note that [D_2] changes by a factor of ~16 for the range of T_F shown. For details, see Ref. [6].

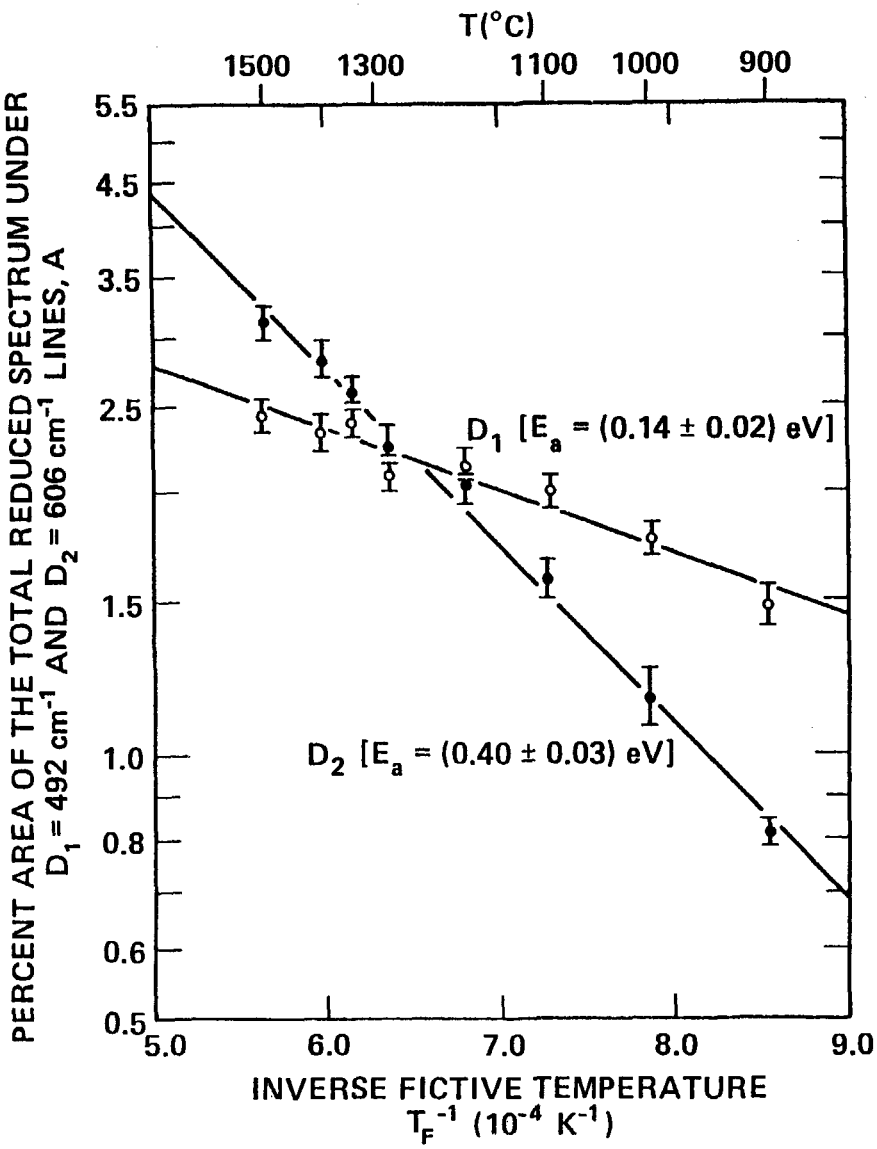

Fig. 7. Semilogarithmic plot of the percent area of the total reduced Raman spectrum under the D_1 (and D_2) peaks vs. $1/T_F$. Points are the mean values of at least four area measurements taken at T_F and the length of an error bar equals two standard deviations of the area measurements at T_F. Straight lines are least-squares fits to Arrhenius behavior; and these determine the energies of formation given.

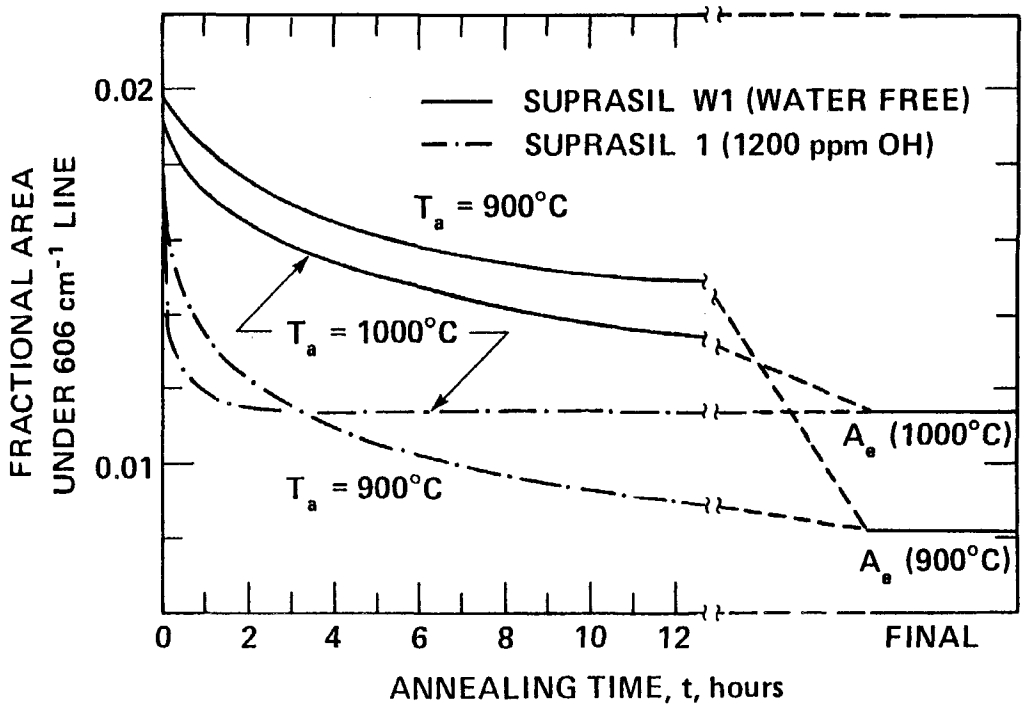

Fig. 8. A schematic illustration of the way that the concentration of D_2 defects decreases with time during annealing at various temperatures T_A. In this example, samples of highly pure (water free) and also of OH containing v-SiO_2 were first annealed to a steady state or equilibrium structure at 1200°C. Then the fractional area A(t) under the D_2 = 606 cm^{-1} line was monitored as a function of the time t spent at a lower annealing temperature T_A. While A(t) decreased more rapidly for samples with high OH content, the final equilibrium concentration A_E was independent of that impurity. The speed of structural relaxation measured by the concentration of D_2 is greatly enhanced by the presence of -OH, and is also faster for higher T_A.

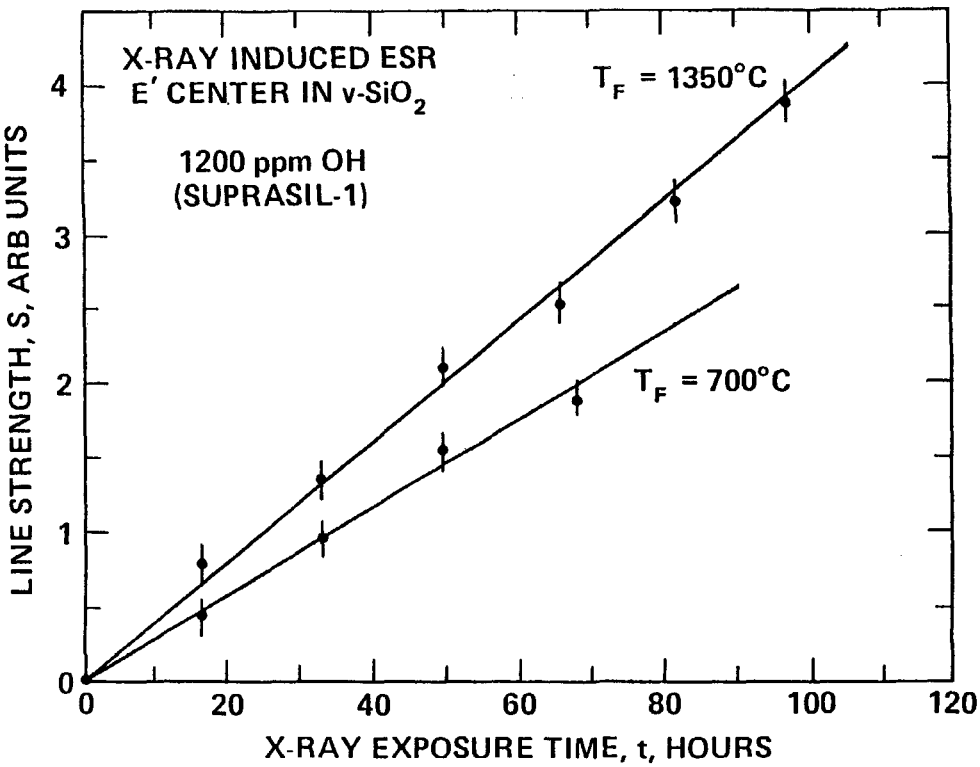

Fig. 9. The strengths S of the E' spin resonance signal as a function of x-ray exposure time t for two samples of "wet" v-SiO_2 preannealed at the different temperatures T_F shown. Radiation hardness increases as T_F is lowered. 100 hours of exposure to the Cu-target x-ray tube equals ~250 Mrad (SiO_2).

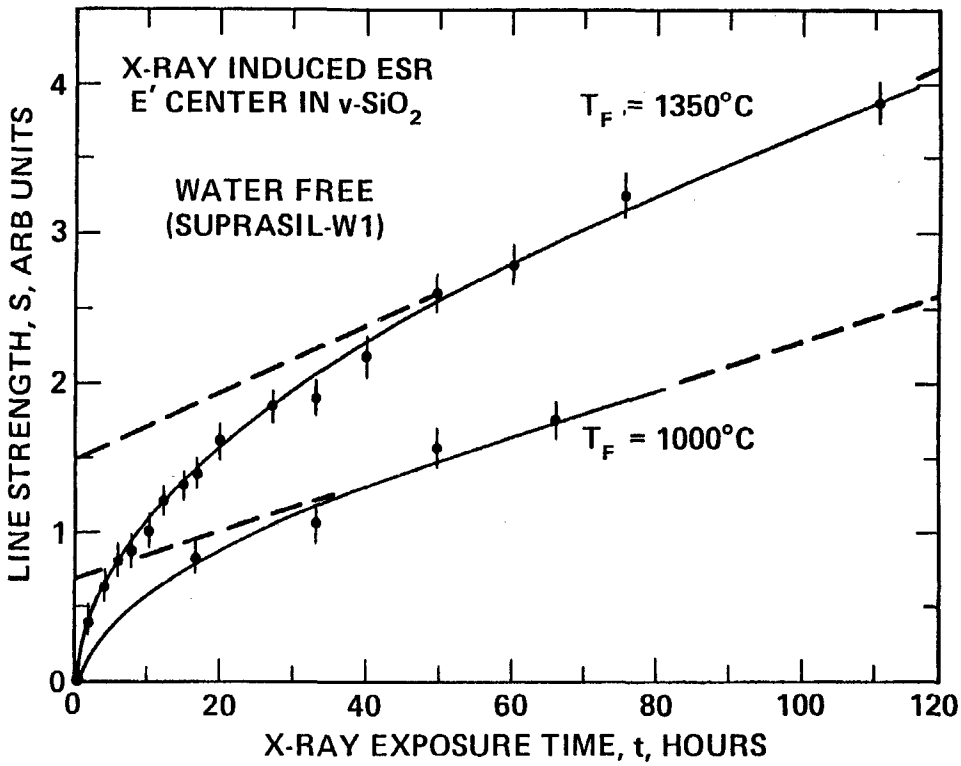

Fig. 10. The strengths S of the E' spin resonance signal vs. x-ray exposure time t for "dry" v-SiO_2 preannealed at *different* T_F. The solid curves are drawn by French curve to aid the eye. The dashed straight line projections to t = 0 give the relative concentration of E' defects existing *before* the irradiation. This increases with T_F in "dry" samples and is much larger than in the "wet" samples shown in Fig. 9.

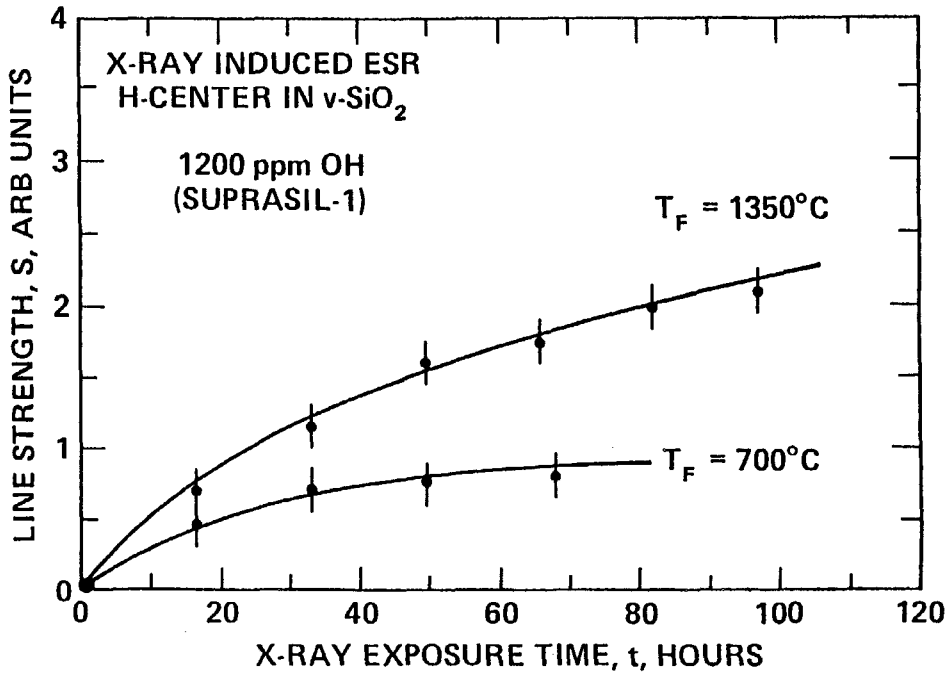

Fig. 11. The strengths S of the ESR signal assigned to the non-bridging oxygen hole center (NBOHC), as a function of x-ray dose for two samples of "wet" vitreous SiO_2, each having a different fictive temperature T_F. The solid curves are drawn to aid the eye.

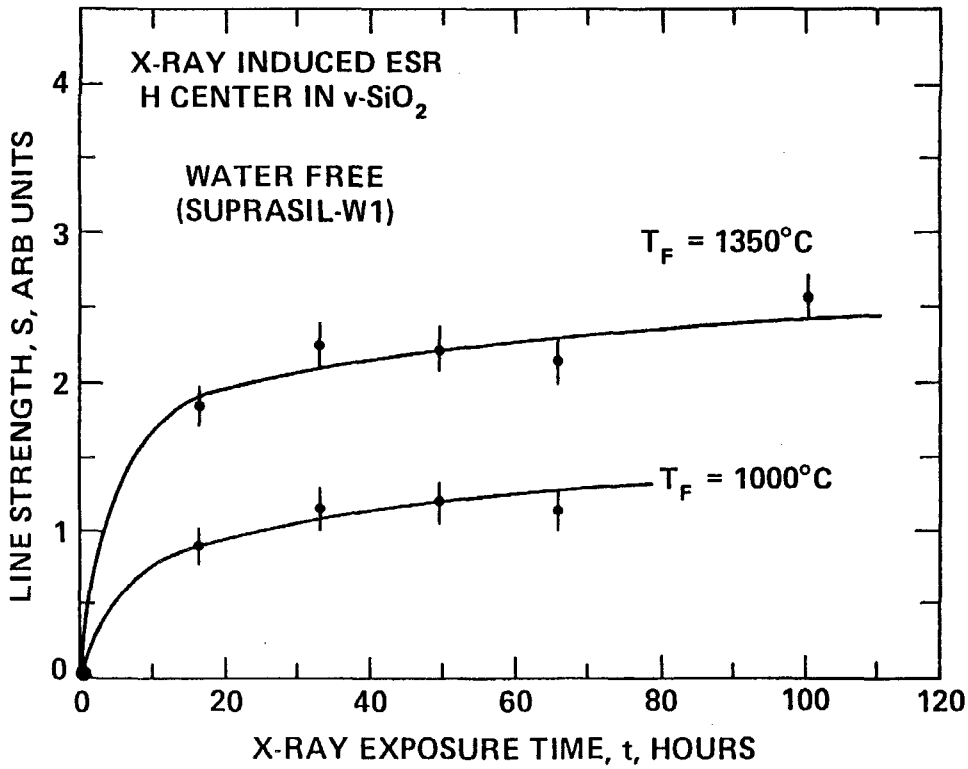

Fig. 12. The strengths S of the ESR signal assigned to the peroxyl radical hole center (PRHC), as a function of x-ray dose for "dry" vitreous SiO_2 samples having two different fictive temperatures T_F. Note the near absence of increase above t ~ 20 hours.

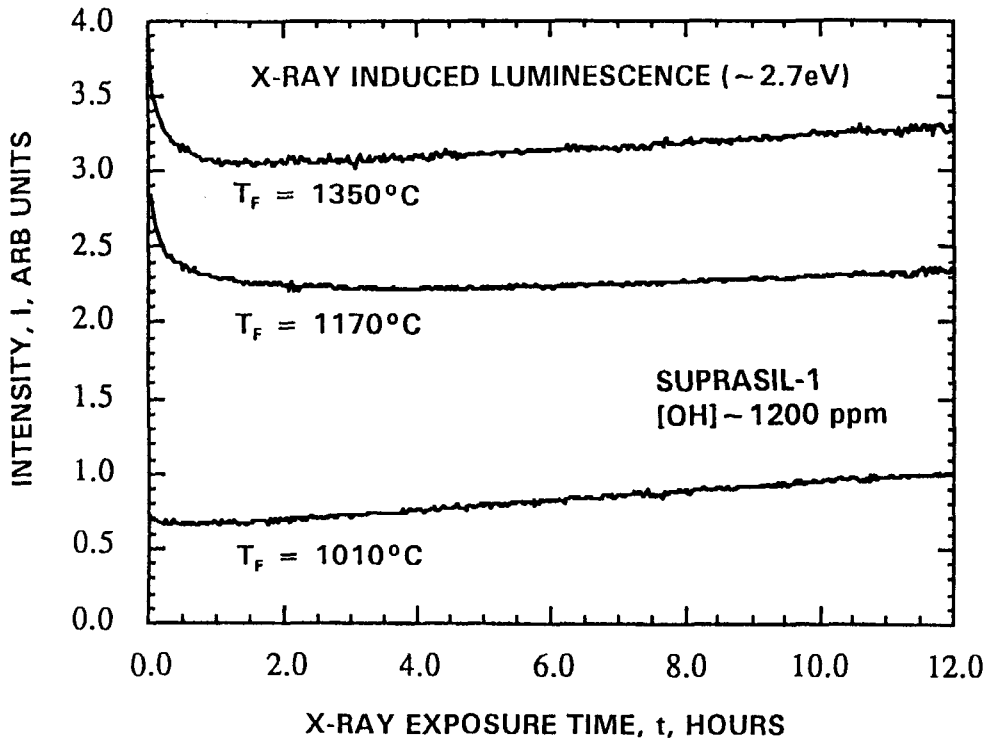

Fig. 13. X-radioluminescence of "wet" v-SiO_2 versus accumulated x-ray dose for different fictive temperatures.

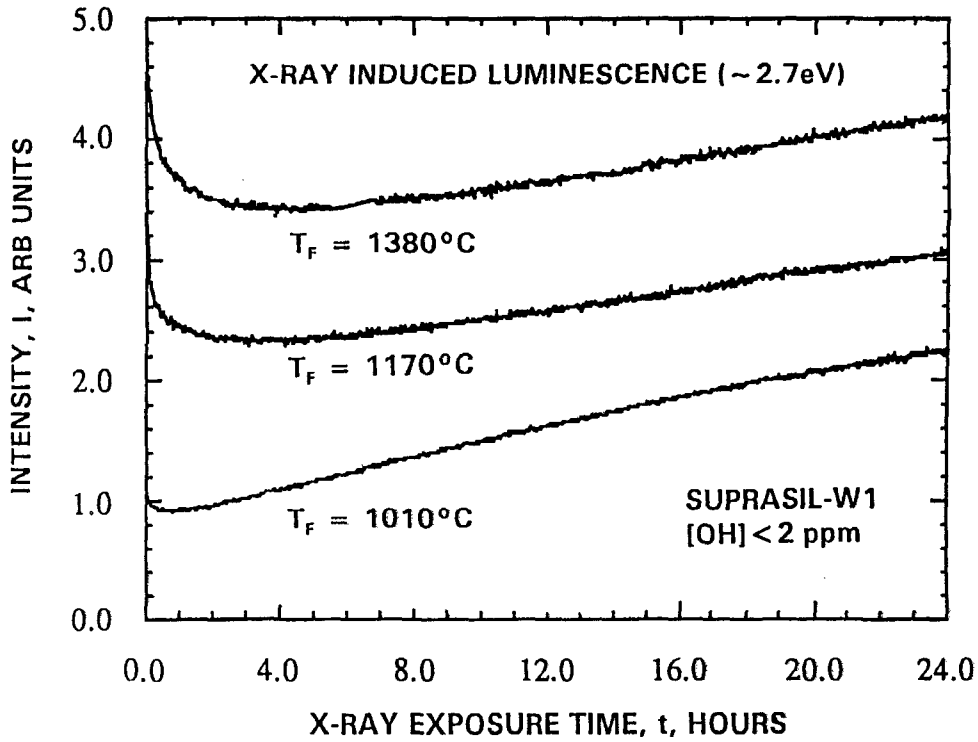

Fig. 14. X-radioluminescence of "dry" v-SiO_2 versus accumulated x-ray dose for different fictive temperatures.